Hindawi
Wireless Communications and Mobile Computing
Volume 2022, Article ID 1961988, 9 pages
https://doi.org/10.1155/2022/1961988

Research Article

The DOA Estimation for a Mixture of Uncorrelated and Coherent Sources via Decomposing the Coprime Array

Heng Jiang, Lichun Li, Mingang Pu, Hailong Zhang, and Xue Li

Information Engineering University, Zhengzhou, Henan 450001, China

Correspondence should be addressed to Heng Jiang; jianghengyx666@163.com

Received 4 July 2022; Revised 23 September 2022; Accepted 20 October 2022; Published 11 November 2022

Academic Editor: Jian Feng Li

The spatial smoothing-based and matrix reconstruction-based decorrelation algorithms are widely used to realize the accurate direction-of-arrival (DOA) estimation with the coexistence of both uncorrelated and coherent sources. However, these methods apply only to the traditional uniform linear array (ULA), of which the manifold matrix is a Vandermonde structure. In this paper, to achieve the DOA estimation of mixed signals on coprime array, the coprime array is decomposed into two independent sub-ULAs, and the received data is processed, respectively. An improved spatial differencing technique is exploited to estimate the uncorrelated and coherent sources separately, and the lost degree of freedom (DOF) caused by array decomposition is recovered. The final high-precision DOA estimation is obtained by conducting an ambiguity resolution method to the estimation results of the decomposed subarrays. Furthermore, double-phase partial spectral search scheme is introduced to diminish the computational complexity. The feasibility and superiority of the proposed algorithm are validated through detailed experimental simulations.

1. Introduction

DOA estimation technology obtains the high-resolution azimuth information of targets through array signal processing, which is widely used in self-driving, medical imaging, seismic survey, and precision attack on battlefield targets [1, 2]. However, coherent sources are frequently found in space due to multipath propagation and malicious smart jammers. In this way, the signal subspace and noise subspace infiltrate each other, and the traditional subspace-based methods might fail since the data covariance matrix is rank-deficient. Therefore, the preprocessing of decorrelation is necessary in these situations.

In accordance with or without the loss of DOF, the mainstream decorrelation algorithms are categorized into dimensionality reduction methods and others. The latter mainly includes Maximum Likelihood (ML) algorithm [3], weighted subspace fitting (WSF) [4], and sparse reconstruction algorithms based on compressed sensing [5]. These methods have broad application scenarios as they demand no correlation of signals and possess high utilization ratio of array antenna. Unfortunately, the multidimensional search and the construction of an overcomplete basis involve huge computational complexity, which seriously prevents them from practical application.

In contrast, the subspace decorrelation methods for dimensionality reduction class have simple models and moderate operands, and are better suited to handle coherent signals. Specifically, spatial smoothing-based algorithm [6] divides the array into a series of overlapping subarrays and restores the rank of matrix by the superposition of subarray covariance. In this way, however, nearly half of the DOF is lost, and only the autocorrelation information of main diagonal accessory entries in the full covariance matrix is exploited, leading to low estimation accuracy. In response, Pillai and Kwon [7] and Grenier and Bosse [8] propose Forward and Backward Spatial Smoothing (FBSS) and Weighted Spatial Smoothing (WSS) algorithms, respectively. An ESPRIT-like decorrelation algorithm termed Single-column Toeplitz (STOEP) method [9] reconstructs a Toeplitz matrix by randomly selecting a column of the covariance matrix. Since the reconstructed matrix of STOEP is insensitive to the coherency between signals, it can also effectively detect coherent signals. And

the Multi-column Toeplitz (MTOEP) method [10] enhances the robustness of STOEP by extracting the complete covariance matrix. To meet the requirement of DOA preinstallation, Zhang et al. [11] further propose

Partial Toeplitz Matrices Reconstruction (PTMR) based on the square of covariance matrix.

To detect more sources and improve the array utilization, Rajagopal and Rao [12] propose the difference algorithm, which exploits the Toeplitz property of the covariance matrix of uncorrelated signals to separate them from the correlated signals and stepwise estimated the DOAs. Furthermore, the papers [13–15] combine oblique projection and matrix transformation for a thorough purge of uncorrelated signals in the difference process.

Nevertheless, all subspace decorrelation algorithms suffer from a strong dependence on the Vandermonde structure of the array manifold, indicating the uniform distribution of physical sensors is required. In practice, the sensors are usually set sparsely to receive more information in a broader space. Since sparse arrays cannot be directly divided into identical overlapping subarrays as uniform arrays do, the spatial transformation processing is inevitable before the decorrelation operation. For instance, Li eta al. [16] and Belloni et al. [17] transformed the sparse planar array into virtual uniform array via array interpolation and manifold separation, respectively, while the signal type and array structure are specially required.

Recently, one representative kind of the sparse array, the coprime array with enhanced DOF and restrained mutual coupling becomes one of the research highlights in array signal processing [18, 19]. The excellent direction-finding performance of coprime array benefits from the construction of an augmented uniform virtual array based on the difference coarray. Distinguished from traditional ULA, however, the reconstructed virtual array is actually equivalent to the single snapshot of second-order statistics, which contains no waveform information of the original signals. Thus, it cannot be applied to the subspace decorrelation algorithm.

To achieve the DOA estimation of coherent signals based on coprime array, the characteristic of prime number is exploited. The coprime array is decomposed into two sparse ULAs with spacing beyond half wavelength. Note the uniform distribution of the decomposed subarrays, the subspace decorrelation algorithms can be extended to it. An optimized spatial differencing method is employed solely for each subarray; the uncorrelated and coherent sources are separated and estimated stepwise. The multiple signal classification (MUSIC) is combined to get the high-accuracy but ambiguous estimation results. Finally, an improved ambiguity resolution algorithm is presented back to the two groups of estimation results, and the unique DOAs are obtained. Although the proposed approach includes two spectrum peak searches, we have opted to discard the global search scheme on MUSIC spectrum in favor of a partial search scheme [20], which reduces the computational cost and guarantees real-time performance in practical applications.

2. System Model

Assume D narrowband quasistationary targets imping on the coprime array with N sensors from the direction of θ_i ($i = 1, 2, \cdots D, \theta_i \in [-\pi/2, \pi/2]$). As depicted in Figure 1, the coprime array is the superposition of a pair of sparse ULAs. Subarray 1 possesses N_1 elements with the spacing of N_2 units, and subarray 2 possesses N_2 elements with the spacing of N_1 units (N_1 and N_2 are coprime numbers, $N_1 < N_2$ and $N_1 + N_2 - 1 = N$). Let d_n represents the location of nth sensors and $\mathbb{S}$ denotes the distribution set. The first marginal element is chosen to be the reference with appropriate generality ($d_1 = 0$).

$$d_n \in \mathbb{S} \cdot d = \{nN_2 d, 0 \le n \le N_1 - 1\} \cup \left\{n' N_1 d, 0 \le n' \le N_2 - 1\right\}. \tag{1}$$

where d is the unit spacing and $d = \lambda/2$, λ denotes the wavelength of the transmitting source.

Suppose there are D_u uncorrelated signals corresponding to the propagation of the independent sources $\boldsymbol{s}_d(t)(d = 1, 2, \cdots, D_u)$ with power $\sigma(d)(d = 1, 2, \cdots, D_u)$; while the rest D_c coherent signals correspond to the propagation of the L groups of coherent sources $\boldsymbol{s}_d(t)$ $(d = D_u + 1, D_u + 2, \cdots, D_u + L)$ with power $\sigma(d)$ $(d = D_u + 1, D_u + 2, \cdots, D_u + L)$. Besides, each coherent group contains p_d multipath signals.

$$D = D_u + D_c = D_u + \sum_{d=D_u+1}^{D_u+L} p_d. \tag{2}$$

The kth $(k = 1, 2, K)$ snapshot $\boldsymbol{x}(k) \in \mathbb{C}^{N\times 1}$ of the received signal is

$$\begin{aligned}
\boldsymbol{x}(k) &= [x_1(k), x_2(k), \cdots, x_N(k)]^T \\
&= \sum_{d=1}^{D_u} \boldsymbol{a}(\theta_d) s_d(k) + \sum_{d=D_u}^{D_u+L} \sum_{l=1}^{p_d} \boldsymbol{a}(\theta_{dl}) \rho_{dl} s_d(k) \\
&= \boldsymbol{A}_u \boldsymbol{s}_u(k) + \boldsymbol{A}_c \boldsymbol{s}_c(k) + \boldsymbol{n}(k) = \boldsymbol{A}\boldsymbol{s}(k) + \boldsymbol{n}(k), \\
\boldsymbol{A} &= [\boldsymbol{A}_u \boldsymbol{A}_c] = \left[\boldsymbol{a}(\theta_1), \boldsymbol{a}(\theta_2), \cdots, \boldsymbol{a}\left(\theta_{D_u}\right), \boldsymbol{a}\left(\theta_{D_u+1}\right), \boldsymbol{a}\left(\theta_{D_u+2}\right), \cdots, \boldsymbol{a}\left(\theta_{D_u+L}\right)\right], \\
\boldsymbol{A}_c &= \left[\boldsymbol{a}\left(\theta_{D_u+1}\right), \boldsymbol{a}\left(\theta_{D_u+2}\right), \cdots, \boldsymbol{a}\left(\theta_{D_u+L}\right)\right] \\
&= \left[\boldsymbol{A}_{D_u+1}\boldsymbol{\rho}_{D_u+1}, \boldsymbol{A}_{D_u+2}\boldsymbol{\rho}_{D_u+2}, \cdots, \boldsymbol{A}_{D_u+L}\boldsymbol{\rho}_{D_u+L}\right] \\
&= \left[\begin{bmatrix} \boldsymbol{a}\left(\theta_{D_u+1,1}\right) \\ \boldsymbol{a}\left(\theta_{D_u+1,2}\right) \\ \vdots \\ \boldsymbol{a}\left(\theta_{D_u+1,p_1}\right) \end{bmatrix}^T \begin{bmatrix} \rho_{D_u+1,1} \\ \rho_{D_u+1,2} \\ \vdots \\ \rho_{D_u+1,p_1} \end{bmatrix}, \cdots, \begin{bmatrix} \boldsymbol{a}\left(\theta_{D_u+L,1}\right) \\ \boldsymbol{a}\left(\theta_{D_u+L,2}\right) \\ \vdots \\ \boldsymbol{a}\left(\theta_{D_u+L,p_L}\right) \end{bmatrix}^T \begin{bmatrix} \rho_{D_u+L,1} \\ \rho_{D_u+L,2} \\ \vdots \\ \rho_{D_u+L,p_L} \end{bmatrix}\right], \\
\boldsymbol{s}(k) &= \begin{bmatrix} \boldsymbol{s}_u^T(k) \\ \boldsymbol{s}_c^T(k) \end{bmatrix} = \begin{bmatrix} \left[s_1(k), s_2(k), \cdots, s_{D_u}(k)\right]^T \\ \left[s_{D_u+1}(k), s_{D_u+2}(k), \cdots, s_{D_u+L}(k)\right]^T \end{bmatrix}, \\
\boldsymbol{a}(\theta_i) &= \left[1, e^{j2\pi d_2 \sin(\theta_i)/\lambda}, \cdots e^{j2\pi d_N \sin(\theta_i)/\lambda}\right]^T, \\
\boldsymbol{n}(k) &= [n_1(k), n_2(k), \cdots n_N(k)]^T,
\end{aligned} \tag{3}$$

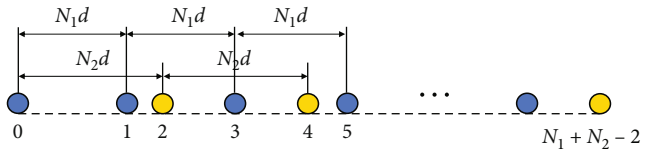

Figure 1: The configuration of the coprime array.

where the $\boldsymbol{A} \in \mathbb{C}^{N\times(D_u+L)}$ is the global manifold matrix, $\boldsymbol{A}_u \in \mathbb{C}^{N\times D_u}$ is the manifold matrix of uncorrelated signals, and $\boldsymbol{A}_c \in \mathbb{C}^{N\times L}$ is the manifold matrix of coherent signals. $\boldsymbol{s} \in \mathbb{C}^{(D_u+L)\times 1}$ denotes the entire signal waveform vector, $\boldsymbol{s}_u \in \mathbb{C}^{D_u\times 1}$ denotes the waveform vector of uncorrelated signals, and $\boldsymbol{s}_c \in \mathbb{C}^{L\times 1}$ denotes the waveform vector of coherent signals. $\boldsymbol{a} \in \mathbb{C}^{N\times 1}$ represents the steering vector and $\boldsymbol{n} \in \mathbb{C}^{N\times 1}$ is the additive Gaussian white noise vector. θ_{dl} and ρ_{dl}, respectively, denotes the DOA and complex attenuation coefficient of the lth $(l = 1, 2, \cdots, p_d)$ multipath signals for the dth $(d = 1, 2, \cdots, L)$ coherent sources.

The sample covariance matrix can be expressed as

$$\begin{aligned}\boldsymbol{R}_{\boldsymbol{xx}} &= E\left[\boldsymbol{x}(k)\boldsymbol{x}(k)^H\right] = \boldsymbol{A}\boldsymbol{R}_{ss}\boldsymbol{A}^H + \sigma_n^2\boldsymbol{I}_N \\ &= \boldsymbol{A}_u\boldsymbol{R}_u{\boldsymbol{A}_u}^H + \boldsymbol{A}_c\boldsymbol{R}_c{\boldsymbol{A}_c}^H + \sigma_n^2\boldsymbol{I}_N,\end{aligned} \tag{4}$$

where $\boldsymbol{R}_u = \mathrm{diag}\left([\sigma_1^2, \sigma_2^2, \sigma_{D_u}^2]\right)$ is the covariance matrix of uncorrelated signals and $\boldsymbol{R}_c = \mathrm{diag}\left([\sigma_{D_u+1}^2, \sigma_{D_u+2}^2, \sigma_{D_u+L}^2]\right)$ denotes the covariance matrix of coherent signals. The global signal covariance matrix $\boldsymbol{R}_{ss}$ is a block diagonal matrix and $\boldsymbol{R}_{ss} = blkdiag(\boldsymbol{R}_u, \boldsymbol{R}_c)$, $\boldsymbol{I}_N$ is the N-dimensional identity matrix.

Limited to the finiteness of snapshot, mathematical average is substituted with statistical average as follows:

$$\bar{\boldsymbol{R}}_{xx} = \frac{1}{K}\sum_{k=1}^{K}\boldsymbol{x}(k)\boldsymbol{x}(k)^H. \tag{5}$$

3. Proposed Method

In this section, the coprime array is decomposed as shown in Figure 2 and a detailed introduction of the proposed method is exhibited. Moreover, the available DOF and computational complexity are analyzed.

3.1. Improved Ambiguity Resolution Algorithm. As is accepted, the phase ambiguity occurs when the interelement spacing of ULA is N' times of the unit spacing, and the real DOAs lost the unique corresponding peaks of the MUSIC spectrum. Considering θ_d as the real DOA and θ_d^a as the corresponding ambiguous angle, the following relationship is satisfied.

$$\sin(\theta_d) - \sin(\theta_d^a) = \frac{2P}{N'}, \tag{6}$$

where the nonzero integer P represents all possible ambiguous angles. If the sensors are spaced no more than half-wavelength apart $(N' \le 1)$, there is no such P fulfills (6) since $|\sin(\theta_d) - \sin(\theta_d^a)| < 2$, and phase ambiguity is absent. If $N' > 1$, in contrast, things can be different. Taking the subarray 1 with $N' \le N_2$ for example, to satisfy (6), we have $|P| < N_2$, and all the possible values of P are $-(N-1), -(N-2), \cdots, -1, 1, \cdots, N-2, N-1$. Since θ_d and θ_d^a are interchangeable, P have $(N_2 - 1)$ possible values, indicating there are N_2 peaks for θ_d including the real peaks. Similarly, there are N_1 peaks in the MUSIC spectrum of the subarray 2 with N_2 sensors, among which only one peak points to the actual DOA.

Since the peak corresponding to real DOA appears at the same position in the spatial spectra of the two coprime subarrays, while the pseudo peaks corresponding to the ambiguous angles do not appear at the same position, the exact unambiguous DOA can be determined by contrasting the estimation results of the subarrays.

φ_n and $\varphi_{n'}$ are chosen to denote the angles set corresponding to the spectral peaks of subarray 1 and subarray 2, respectively. Then, the estimation results of the two subarrays, $\widehat{\varphi}_n$ and $\widehat{\varphi}_{n'}$, are resolved by

$$(\widehat{\varphi}_n, \widehat{\varphi}_{n'}) = \min_{\varphi_n,\varphi_{n'}} |\varphi_n - \varphi_{n'}| \left(n = 1, 2, \cdots, N_2, n' = 1, 2, \cdots, N_1\right). \tag{7}$$

To acquire the signal information in a wider range and improve the estimation accuracy, the estimation results of the subarray with larger aperture are selected as the final DOA estimation result

$$\widehat{\theta}_i = \begin{cases} \widehat{\varphi}_n & (N_1 - 1)N_2 \ge (N_2 - 1)N_1, \\ \widehat{\varphi}_{n'} & (N_1 - 1)N_2 < (N_2 - 1)N_1. \end{cases} \tag{8}$$

3.2. The Estimation of Uncorrelated Sources. The MUSIC algorithm is exploited to estimate the uncorrelated signals first. The Eigendecomposition (EVD) of the whole covariance matrix $\boldsymbol{R}$ is expressed as

$$\boldsymbol{R} = U\boldsymbol{\Sigma}U^H = U_s\boldsymbol{\Sigma}_s{U_s}^H + U_n\boldsymbol{\Sigma}_n{U_n}^H, \tag{9}$$

where $\boldsymbol{\Sigma} = \mathrm{diag}\left([\lambda_1, \lambda_2, \lambda_{N_1}]\right)$ is the diagonal matrix of eigenvalues and $\lambda_1 \ge \lambda_2 \ge \cdots \ge \lambda_{D_u+L} \ge \lambda_{D_u+L+1} = \cdots = \lambda_{N_1}$. $\boldsymbol{\Sigma}_s = \mathrm{diag}\left([\lambda_1, \lambda_2, \lambda_{D_u+L}]\right)$ consists of signal eigenvalues, and $\boldsymbol{\Sigma}_n = \mathrm{diag}\left([\lambda_{D_u+L+1}, \lambda_{D_u+L+2}, \lambda_{N_1}]\right)$ comprises the noise eigenvalues. $\boldsymbol{U} = [\boldsymbol{U}_s, \boldsymbol{U}_n]$, $\boldsymbol{U}_s$, and $\boldsymbol{U}_n$ are the matrixes whose columns are the corresponding eigenvectors of $\boldsymbol{\Sigma}_s$ and $\boldsymbol{\Sigma}_n$.

Given that the signal subspace $\boldsymbol{U}_s$ and the noise subspace $\boldsymbol{U}_n$ are orthogonal, and the steering vectors span the same vector space as $\boldsymbol{U}_s$ do, therefore,

$$\left|\boldsymbol{a}(\theta_d)^H\boldsymbol{U}_n\right|^2 = 0 \; d = 1, 2, D_u, \tag{10}$$

$$\left|(\boldsymbol{A}_d\boldsymbol{\rho}_d)^H\boldsymbol{U}_n\right|^2 = 0 \; d = D_u + 1, D_u + 2, D_u + L. \tag{11}$$

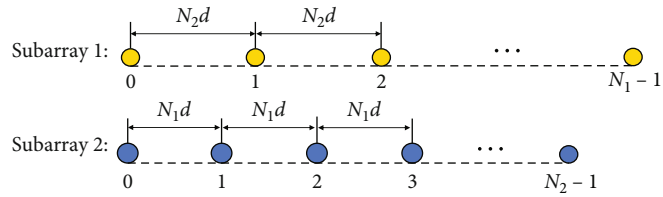

Figure 2: The diagrammatic sketch of the decomposed coprime subarray.

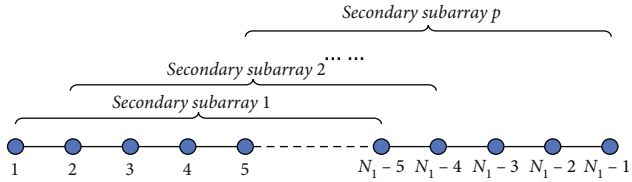

Figure 3: The partition of secondary subarrays.

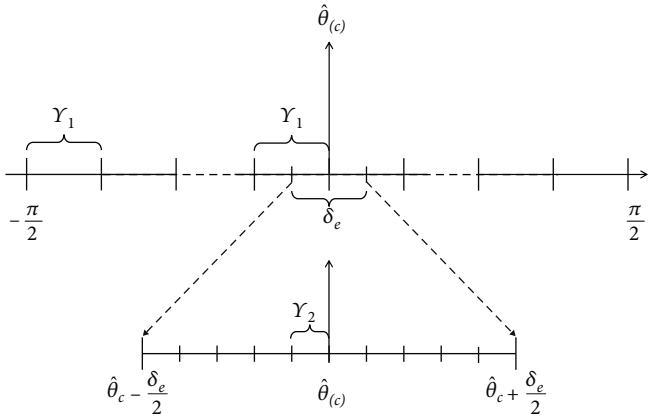

Figure 4: Biorder partial spectral search scheme.

Since $\boldsymbol{A}_d\boldsymbol{\rho}_d$ is the linear combination of the column vector of a Vandermonde matrix, the steering vectors of the single multiple signals in each coherent group cannot satisfy Equation (10) like that of uncorrelated signals. Consequently, the DOAs of the uncorrelated sources can be obtained by searching the peaks of

$$f(\theta)=\frac{1}{\boldsymbol{a}(\theta)^H\boldsymbol{U}_n\boldsymbol{U}_n{}^H\boldsymbol{a}(\theta)}. \tag{12}$$

After obtaining the estimation results on the two subarrays, the unique DOAs of unrelated signals are obtained by applying the ambiguity resolution algorithm shown in Section 3.1.

3.3. The Estimation of Coherent Sources. In this section, an improved spatial differencing method [14] is used to eliminate the uncorrelated components in the covariance matrix, and the estimation of coherent signals is possessed by the differencing matrix.

As demonstrated in Figure 3, subarray 1 is further divided into p overlapping identical secondary subarrays, each of which has (N_1-p+1) elements and the spacing of N_2d.

The covariance matrix of the mth$(m=1,2,\cdots,p)$ secondary subarray $\boldsymbol{R}_m\in\mathbb{C}^{(N_1-p+1)}$ meets the following expression:

$$\boldsymbol{R}_m=\boldsymbol{K}_m\boldsymbol{R}\boldsymbol{K}_m{}^H, \tag{13}$$

where the selection matrix $\boldsymbol{K}_m\in\mathbb{C}^{(N_1-p+1)\times N_1}$ is given by

$$\boldsymbol{K}_m=\left[\boldsymbol{0}_{(N_1-p+1)\times(m-1)},\boldsymbol{I}_{(N_1-p+1)},\boldsymbol{0}_{(N_1-p+1)\times(p-m)}\right]. \tag{14}$$

To dissociate the coherent sources from uncorrelated signals and resolve the rank deficiency, the equivalent spatial smoothing is performed by averaging the difference between $\boldsymbol{R}_1$ and $\boldsymbol{R}_m(m=1,2,\cdots,p)$.

$$\boldsymbol{D}_p=\frac{1}{p}\sum_{m=1}^{p}\left(\boldsymbol{R}_1-\boldsymbol{J}_{N_1-p+1}\boldsymbol{R}_m{}^*\boldsymbol{J}_{N_1-p+1}\right), \tag{15}$$

where $\boldsymbol{J}_{N_1-p+1}$ is the (N_1-p+1) dimensional antidiagonal matrix and the pth order spatial differencing matrix $\boldsymbol{D}_p$ owns the following essential properties: (1) only the information of coherent components is remained in $\boldsymbol{D}_p$. (2) The rank of $\boldsymbol{D}_p$ equals to the total number of coherent sources D_c $(\text{rank}\ (\boldsymbol{D}_p)=D_c)$ when $(p\geq\max p_d(d=D_u+1,D_u+2,D_u+L))$ and $(N_1-p+1>D_c=D\overset{d}{-}D_u)$. Detailed proof can be found in [14].

$\boldsymbol{D}_p$ is Eigen decomposed as

$$\boldsymbol{D}_p=U_{\text{ps}}\boldsymbol{\Sigma}_{\text{ps}}U_{\text{ps}}{}^H+U_{\text{pn}}\boldsymbol{\Sigma}_{\text{pn}}U_{\text{pn}}{}^H, \tag{16}$$

where $\boldsymbol{\Sigma}_{ps}=\text{diag}\ ([\lambda_1,\lambda_2,\lambda_{D_c}])$ is the diagonal matrix of signal eigenvalues, $\boldsymbol{\Sigma}_{\text{pn}}=\text{diag}\ ([\lambda_{D_c+1},\lambda_{D_c+2},\lambda_{N_1-p+1}])$ is the diagonal matrix of noise eigenvalues. $\boldsymbol{U}_{\text{ps}}$ and $\boldsymbol{U}_{\text{pn}}$ are the subspaces composed of the corresponding eigenvectors of signal eigenvalues and noise eigenvalues, respectively. According to the orthogonality of the steering vectors and the noise subspace, the coherent signals can be detected by searching the spectrum peaks of:

$$\begin{gathered}f(\theta_{\text{dl}})\triangleq\left|\boldsymbol{a}^H(\theta_{\text{dl}})\boldsymbol{U}_{\text{pn}}\right|^2=0\\ \forall d\in[D_u+1,D_u+2,\cdots,D_u+L],\forall l\in[1,2,\cdots,p_d]\end{gathered}. \tag{17}$$

Next, the ambiguity resolution algorithm is used again to get the unique DOAs of coherent signals.

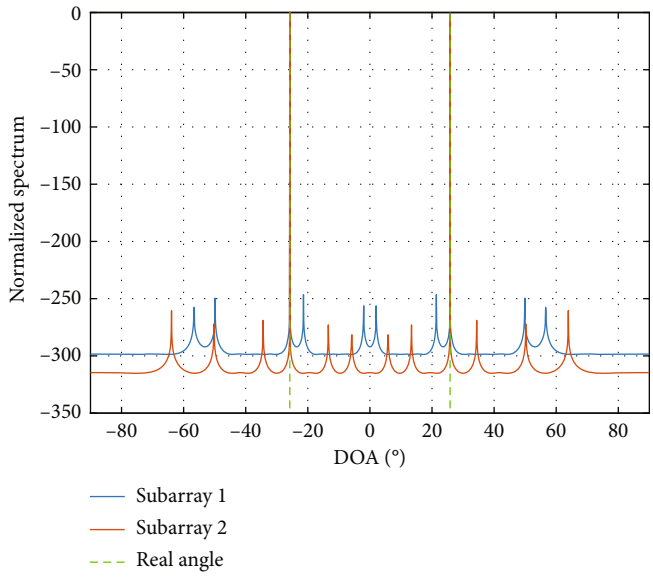

Figure 5: Normalized spectrum of uncorrelated signals.

3.4. Biorder Partial Spectral Search Scheme. Since the proposed algorithm involves two spectral peak searches, the selection of search step Υ is crucial: the computational complexity is expensive when Υ is small, while the estimation accuracy will decrease when Υ goes higher. The biorder partial spectral search scheme [21] is introduced to improve the precision without costing much computational complexity. As shown in Figure 4, the first search is performed with initial step size Υ_1 to obtain a roughly estimated angle $\widehat{\theta}_{(c)}$, and then the second search is performed during the range of $[\widehat{\theta}_{(c)} - \delta_e/2, \widehat{\theta}_{(c)} + \delta_e/2]$ with step size Υ_2 ($\Upsilon_2 = \Upsilon_1/10$) to obtain the refined estimated angle $\widehat{\theta}$.

The detailed steps of the proposed algorithm are listed as follows:

(1) The received data of subarray 1 is collected and the covariance matrix $\boldsymbol{R}^1$ is calculated via Equation (5)

(2) $\boldsymbol{R}^1$ is eigendecomposed to plot the spatial spectrum of uncorrelated signals via Equation (12). The biorder partial spectral search scheme is applied to find the ambiguous DOAs of the uncorrelated signals

(3) The pth order spatial differencing matrix $\boldsymbol{D}_p$ is generated via Equation (15).

(4) $\boldsymbol{D}_p$ is eigendecomposed to plot the spatial spectrum of uncorrelated signals via Equation (17). And the biorder partial spectral search scheme is applied again to find the ambiguous DOAs of the coherent signals

(5) Steps 1-4 are repeated on subarray 2 to obtain the ambiguous estimation results of the uncorrelated sources and coherent sources

(6) The results of the two subarrays are deblurred via Equations (7) and (8) to attain the unique DOAs

3.5. DOF. Since $N_1 < N_2$, the maximum number of detectable sources, namely the DOF, is depending on subarray 1. To correctly identify the uncorrelated sources using MUSIC algorithm, the signal subspace cannot fulfill the eigenspace and the demanded condition is presented as

$$D_u + L < N_1. \tag{18}$$

For the same reason,

$$D_c = \sum_{d=1}^{L} p_d < N_1 - p + 1, \tag{19}$$

when $p = \max_d p_d = 2$, $D_c = 2L < N_1 - 1$, and the maximum value of L ($L_{\max}$) equals to $\lfloor (N_1 - 2)/2 \rfloor = \lfloor N_1/2 \rfloor - 1$. Then,

$$(D_c)_{\max} = 2L_{\max} = \lfloor N_1 \rfloor - 2. \tag{20}$$

$L_{\max}$ is substituted into Equation (18) as follows:

$$(D_u)_{\max} = N_1 - L - 1 = N_1 - \lfloor N_1/2 \rfloor + 1 - 1 = \lceil N_1/2 \rceil. \tag{21}$$

Combining Equation (20) with Equation (21), the DOF of the proposed method is derived as

$$\mathrm{DOF} = (D_u)_{\max} + (D_c)_{\max} = \lfloor 3N_1/2 \rfloor - 2. \tag{22}$$

3.6. Computational Complexity. The computational complexity of the proposed algorithm is investigated in this section, which mainly focuses on the eigenvalue decomposition and spectral peak search.

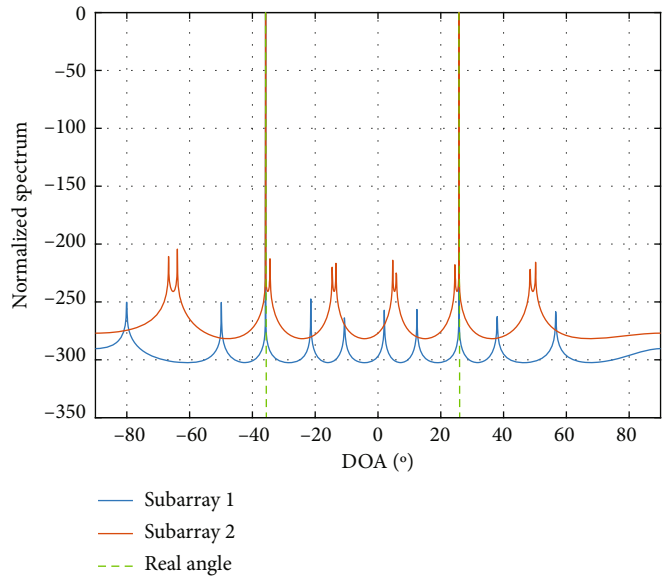

Figure 6: Normalized spectrum of coherent signals.

Subarray 1 is considered first. For the estimation of uncorrelated signals, the computational complexity of EVD of covariance matrix $\boldsymbol{R} \in \mathbb{C}^{N_1 \times N_1}$ is $O((N_1)^3)$, and the computational complexity of the peak-finding searching is $O((N_1)^2 G_u)$. Here the $G_u = G_{u1} + G_{u2}$ is the total number of search points, which is inversely proportional to search step Υ. $G_{u1} = 180 \circ / \Upsilon_1$ and $G_{u2} = D_u N_2 \delta_e / \Upsilon_2$ are the search points of the rough search and refined search, respectively. For the estimation of coherent signals, the computational complexity of EVD of spatial differencing matrix $\boldsymbol{D}_p \in \mathbb{C}^{(N_1-p+1)\times(N_1-p+1)}$ is $O((N_1 - p + 1)^3)$, and the computational complexity of the peak-finding searching is $O((N_1 - p + 1)^2 G_c)$ and $G_c = 180 \circ / \Upsilon_1 + D_c N_2 \delta_e / \Upsilon_2$. Hence, the computational complexity of subarray 1 is concluded as $O((N_1)^3 + (N_1 - p + 1)^3 + (N_1)^2 G_u + (N_1 - p + 1)^2 G_c)$. Similarly, the computational complexity of subarray 2 is $O((N_2)^3 + (N_2 - p + 1)^3 + (N_2)^2 G_u{}' + (N_2 - p + 1)^2 G_c{}')$, $G_u{}' = 180 \circ / \Upsilon_1 + D_u N_1 \delta_e / \Upsilon_2$, and $G_c{}' = 180 \circ / \Upsilon_1 + D_c N_1 \delta_e / \Upsilon_2$. The total computational complexity is calculated as follows:

$$O\Big((N_1)^3 + (N_2)^3 + (N_1 - p + 1)^3 + (N_2 - p + 1)^3 + (N_1)^2 G_u + (N_2)^2 G_u{}' + (N_1 - p + 1)^2 G_c + (N_2 - p + 1)^2 G_c{}'\Big). \tag{23}$$

4. Simulation Results

In this section, the effectiveness of the ambiguity resolution algorithm is verified, and the comparisons of the computational complexity and DOA performance are presented. Suppose the coprime array has a total of 10 sensors, which is decomposed to the five-element subarray 1 with the spacing of $6d$, and the six-element subarray 2 with the spacing of $5d (N = 10, N_1 = 5, N_2 = 6)$.

4.1. Experiment 1: Ambiguity Resolution Algorithm. Assume that two coherent signals come from $\theta_{1,1} = -25.8 \circ$ and $\theta_{1,2} = 25.8 \circ$ with the complex attenuation coefficient of $(1 + 0.3i)$ and $(1 + 0.5i)$, respectively. Furthermore, there are two uncorrelated signals at $\theta_2 = -35.8 \circ$ and $\theta_3 = 25.8 \circ$. The Signal to Noise Ratio (SNR) is set to be $SNR = 10$dB, and the snapshot $K = 500$.

The MUSIC spectrums in Equation (12) for both uncorrelated signals and coherent signals are shown in Figures 5 and 6. Note that there are 12 $(D_u N_2 = 2 \times 6 = 12)$ peaks presented in the spectrum corresponding to subarray 1, and 10 $(D_u N_1 = 2 \times 5 = 10)$ peaks corresponding to subarray 2, which is identical to the theory in Section 3.1.

The reason why peaks outnumber sources is the existence of ambiguity. Due to the characteristic of prime numbers, only the spectral peaks corresponding to the real DOA θ_d present in the same position of both MUSIC spectrums, while the spectral peaks corresponding to θ_d^{α} do not. Hence, the unique DOAs can be derived by finding the overlapping peaks. The proposed algorithm can accurately detect all four signals as exhibited in Table 1, where the red marks represent the overlapping angles of the two subarrays, namely the estimated results.

Furthermore, by estimating uncorrelated signals and coherent signals separately, it can break through the resolution limit of conventional spatial spectrum estimation algorithms and detect two distinct signals from the same angle.

4.2. Experiment 2: Computational Complexity. To reflect the advantages of the biorder partial spectral search strategy, the computational complexity of regular spectral searching method (RSS) is compared with the proposed search strategy $(\Upsilon_1 = 0.1, \Upsilon_2 = 0.01, \delta_e = \Upsilon_1)$ versus different numbers of sensors.

Table 1: the Angle values corresponding to spectrum peaks.

	Subarray 1	Subarray 2
Uncorrelated sources	-56.64°, -25.80°, -2.02°, 2.02°, 25.80°, 56.64°	-63.91°-25.80°, 3.042°, 25.80°, 63.91°
Coherent sources	-80.05°, -35.80°, -10.66°, 2.02°, 25.80°, 56.64°	-66.68°, -63.91°, -35.80°, 25.80°, 48.45°

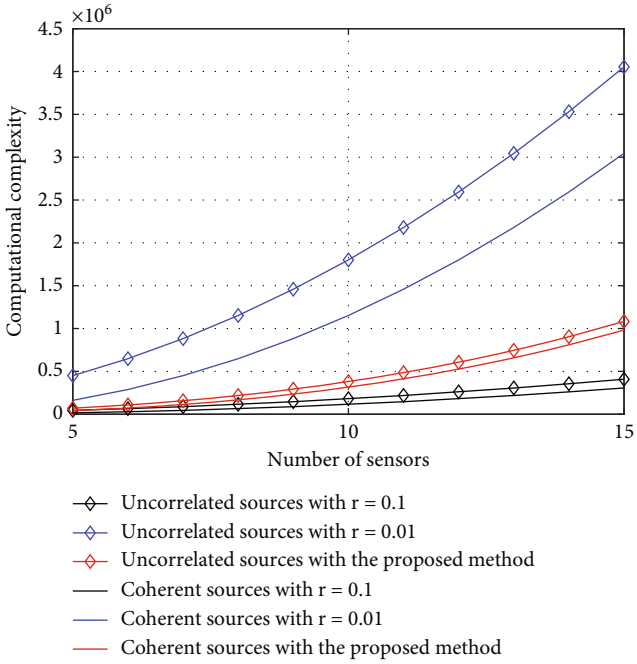

Figure 7: Comparison of computational complexity.

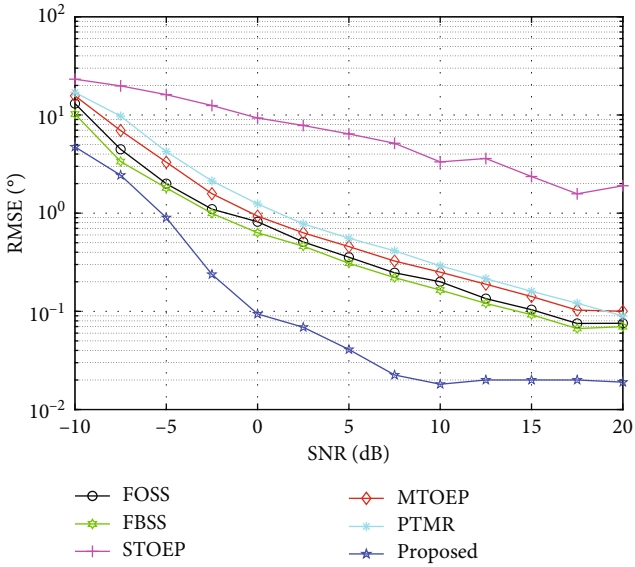

Figure 8: The RMSE curves versus SNR.

As can be seen from the comparison in Figure 7, the computational complexity of the optimized searching strategy, the red line lines, is much lower than that of rough RSS ($\Upsilon = 0.1$) and close to that of fine RSS ($\Upsilon = 0.01$), no matter for coherent signals or uncorrelated signals. Since the accuracy of the subspace MUSIC algorithm depends on the length of searching step, the simulation results reveal that the biorder search strategy can maintain precise DOA estimation results while taking into account the computational complexity.

4.3. Experiment 3: The Performance of DOA Estimation. The forward spatial smoothing (FOSS [6]), forward-backward spatial smoothing (FBSS [7]), Single Toeplitz method (STOEP [9]), Multiple Toeplitz method (MTOEP [10]), and Partial Toeplitz square Matrix Reconstruction (PTMR [11]) are compared with the proposed algorithm. Root mean square error (RMSE) and the estimation accuracy (Acc) are chosen to reflect the magnitude of angle estimation bias, which is defined as follows:

$$RMSE = \sqrt{\frac{1}{DW}\sum_{d=1}^{D}\sum_{w=1}^{W}(\theta_{d,w} - \theta_d)}, \qquad Acc = \frac{F_r}{DW} \times 100\%, \tag{24}$$

where W is the number of Monte Carlo simulations, $\theta_{d,w}$ denotes the estimation angle of θ_d in the wth Monte Carlo simulation, and F_r counts all occurrences of $|\theta_{d,w} - \theta_d| < 0.5\circ$. For the coprime array, $M = 7, N = 6$. Assume three sources imping on the antenna array from $[0\circ, 25.8\circ, 40\circ]$, of which the first two sources are coherent sources with complex attenuation coefficients of $[1 + 0.3i, 1 + 0.5i]$, and the last source is independent from other sources. 1000 Monte Carlo trials are repeated to eliminate the randomness of the data.

4.3.1. DOA Performance versus SNR. The number of snapshots is set to be 200 and SNR is evenly evaluated at intervals of 2.5 within the range of −10 ~ 20. The performance comparisons of RMSE and Acc versus different SNRs are exhibited in Figures 8 and 9.

Consistent with expectations, with the increase of SNR, the RMSE gradually decreases and the Acc gradually increases. It is evident that the blue stars line always corresponds to the lowest RMSE and the highest Acc, indicating that the proposed algorithm outperforms the others. Although the reconstruction of full-rank covariance is simpler for matrix reconstruction-based decorrelation algorithms, the reconstructed noise power becomes the square of original noise power, thus the DOA performance of MTOEP is inferior to FOSS and FBSS.

In contrast, although the proposed algorithm loses nearly half of the array DOF due to the decomposition of coprime array, spatial differencing technique is employed

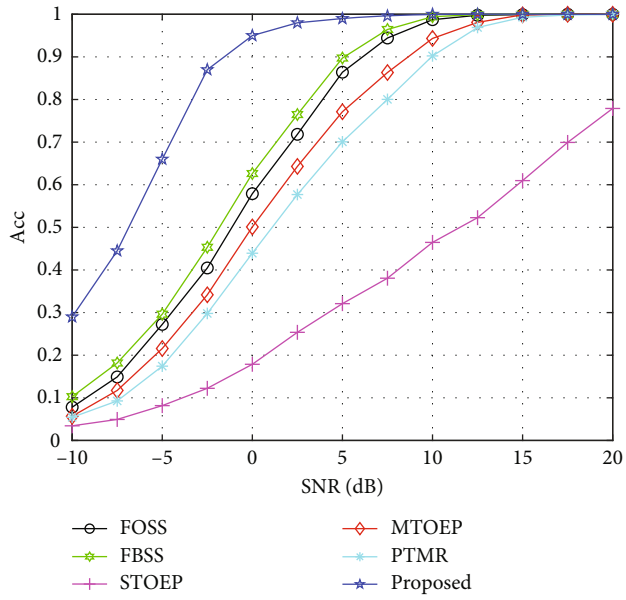

Figure 9: The Acc curves versus SNR.

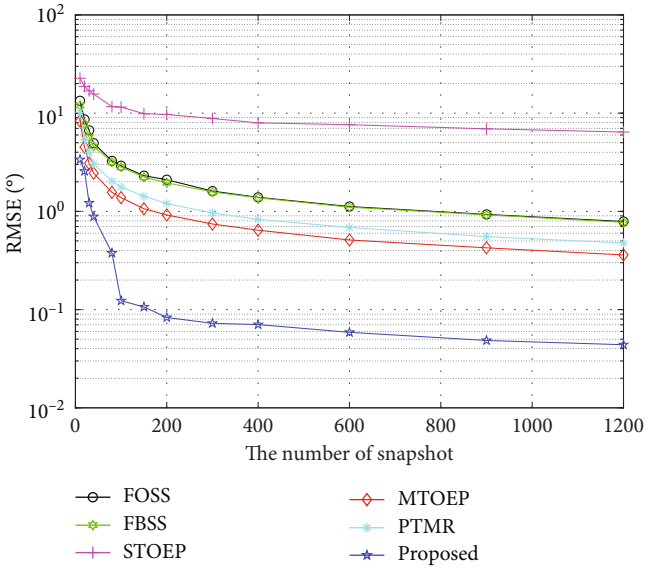

Figure 10: The comparison of RMSE versus snapshot number.

to recoup this loss by estimating the uncorrelated sources and coherent sources in two consecutive steps. Compared with other algorithms with the same DOF, the proposed algorithm can obtain signal information in a larger range and effectively suppress the mutual coupling due to sparse layouts of array sensors, hence achieving the optimum DOA estimation performance.

4.3.2. DOA Performance versus Snapshot Number. The number of snapshots is another crucial factor to determine the DOA performance except for SNR. As shown in Figures 10 and 11, Monte Carlo experiments study the comparison of RMSE and Acc versus different snapshot numbers ($K = [10$, 20, 30, 40, 80, 100, 150, 200, 300, 400, 600, 900, 1200]). The SNR is fixed at 0 dB, and other experimental parameters remain unchanged.

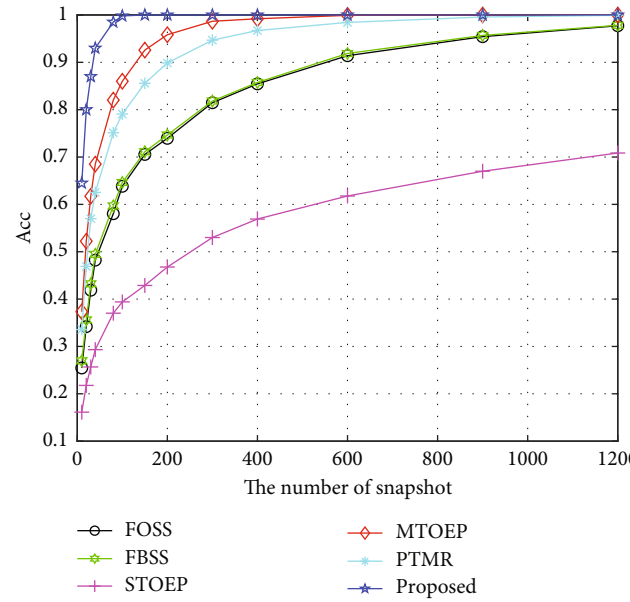

Figure 11: The comparison of Acc versus snapshot number.

As demonstrated above, the performance curve of the RMSE is continuing to decline with the addition of snapshots. Apparently, the proposed algorithm can obtain the lowest RMSE and the highest Acc for each snapshot number. The proposed algorithm can reduce RMSE to the level of nearly zero and achieve an accurate rate of approximately 100% with only 100 snapshots.

5. Conclusion

In this paper, the joint estimation of both uncorrelated and coherent sources on sparse array is achieved based on the decomposed coprime subarrays and spatial differencing technique. Since uncorrelated and coherent sources are estimated separately, the number of detectable sources exceeded that of physical sensors; even two sources from the same azimuth can be distinguished for some specific situations. Furthermore, the biorder search strategy is introduced to reduce computational complexity. The available DOF is calculated and computational complexity is analyzed. Exhaustive simulations confirm the superior performance of the proposed approach under harsh conditions with limited snapshots and low SNR.

Data Availability

The data used to support the findings of this study are included within the article.

Conflicts of Interest

The authors declare that they have no conflicts of interest.

References

[1] A. Patwari, *Sparse Linear Antenna Arrays: A Review*, Antenna System, 2021.

[2] H. Jiang, L. Li, and X. Li, "GSNA: a novel sparse array design achieving enhanced degree of freedom for noncircular sources," *Wireless Communications and Mobile Computing*, vol. 2022, Article ID 2950166, 9 pages, 2022.

[3] F. Vincent, O. Besson, and E. Chaumette, "Approximate unconditional maximum likelihood direction of arrival estimation for two closely spaced targets," *IEEE Signal Processing Letters*, vol. 22, no. 1, pp. 86–89, 2015.

[4] D. Meng, X. Wang, M. Huang, L. Wan, and B. Zhang, "Robust weighted subspace fitting for DOA estimation via block sparse recovery," *IEEE Communications Letters*, vol. 24, no. 3, pp. 563–567, 2020.

[5] Y. Wang, X. Yang, J. Xie, L. Wang, and B. W. H. Ng, "Sparsity-inducing DOA estimation of coherent signals under the coexistence of mutual coupling and nonuniform noise," *IEEE Access*, vol. 7, pp. 40271–40278, 2019.

[6] J. E. Evans, J. R. Johnson, and D. F. Sun, *High Resolution Angular Spectrum Estimation Techniques for Terrain Scattering Analysis and Angle of Arrival Estimation*, IEEE ASSP Workshop Spectral Estimate, 1981.

[7] S. U. Pillai and B. H. Kwon, "Forward/backward spatial smoothing techniques for coherent signal identification," *IEEE Transactions on Acoustics, Speech, and Signal Processing*, vol. 37, no. 1, pp. 8–15, 1989.

[8] D. Grenier and E. Bosse, "Decorrelation performance of DEESE and spatial smoothing techniques for direction-of-arrival problems," *IEEE Transactions on Signal Processing*, vol. 44, no. 6, pp. 1579–1584, 1996.

[9] F. M. Han and X. D. Zhang, "An ESPRIT-like algorithm for coherent DOA estimation," *IEEE Antennas and Wireless Propagation Letters*, vol. 4, pp. 443–446, 2005.

[10] W. Zhang, Y. Han, and M. Jin, "Toeplitz matrices reconstruction based DOA estimation for coherent signals," *Journal of Jilin University (Engineering and Technology Edition)*, vol. 50, no. 2, p. 8, 2020.

[11] W. Zhang, Y. Han, M. Jin, and X. S. Li, "An Improved ESPRIT-like Algorithm for Coherent Signals DOA Estimation," *IEEE Communications Letters*, vol. 24, no. 2, pp. 339–343, 2019.

[12] R. Rajagopal and P. R. Rao, "Generalised algorithm for DOA estimation in a passive sonar," *IEE Proceedings F Radar and Signal Processing*, vol. 140, no. 1, pp. 12–20, 1993.

[13] W. Sun, B. Jianlin, and K. Wang, "Novel method of ordinal bearing estimation for more sources based on oblique projector," *Journal of Systems Engineering and Electronics*, vol. 20, no. 3, pp. 445–449, 2009.

[14] F. Liu, J. Wang, C. Sun, and R. Du, "Spatial differencing method for DOA estimation under the coexistence of both uncorrelated and coherent signals," *IEEE Transactions on Antennas & Propagation*, vol. 60, no. 4, pp. 2052–2062, 2012.

[15] X. Ma, X. Dong, and Y. Xie, "An improved spatial differencing method for DOA estimation with the coexistence of uncorrelated and coherent signals," *IEEE Sensors Journal*, vol. 16, no. 10, pp. 3719–3723, 2016.

[16] L. I. Yuanji, N. Wang, B. Zeng, Y. Yang, and J. Sun, "DOA estimation of coherent sources based on virtual Array of 2-dimension sparse Array," *Modern Radar*, vol. 40, no. 5, p. 5, 2018.

[17] F. Belloni, A. Richter, and V. Koivunen, "DoA estimation via manifold separation for arbitrary array structures," *IEEE Transactions on Signal Processing*, vol. 55, no. 10, pp. 4800–4810, 2007.

[18] P. Pal and P. P. Vaidyanathan, "Coprime sampling and the MUSIC algorithm," in *2011 Digital Signal Processing and Signal Processing Education Meeting (DSP/SPE)*, pp. 289–294, Sedona, AZ, USA, 2011.

[19] C. L. Liu, P. P. Vaidyanathan, and P. Pal, "Coprime coarray interpolation for DOA estimation via nuclear norm minimization," in *IEEE International Symposium on Circuits & Systems*, pp. 2639–2642, Montreal, QC, Canada, 2016.

[20] F. Sun, B. Gao, and L. Peng, "Partial spectral search-based DOA estimation method for co-prime linear arrays," *Electronics Letters*, vol. 51, no. 24, pp. 2053–2055, 2015.

[21] C. Zhou, Z. Shi, Y. Gu, and X. Shen, "DECOM: DOA estimation with combined MUSIC for coprime array," in *International Conference on Wireless Communications & Signal Processing*, pp. 1–5, Hangzhou, China, 2013.